Journal of Magnetics 11(1), 30-35 (2006)

Microstructure and Magnetic Characteristics of Mn-doped Finemet Nanocomposites

Anh-Tuan Le[1], Chong-Oh Kim[1], Nguyen Chau[2], Nguyen Duc Tho[2], Nguyen Quang Hoa[2], and Heebok Lee[3]*

[1]*Research Center for Advanced Magnetic Materials, Chungnam National University, Taejon 305-764, Korea*
[2]*Center for Materials Science, National University of Hanoi, 334 Nguyen Trai, Hanoi, Vietnam*
[3]*Department of Physics Education, Kongju National University, Kongju 314-701, Korea*

(Received 14 November 2005)

A thorough study about the influences of Mn substitution for Fe on the microstructure and magnetic characteristics of $Fe_{73.5-x}Mn_xSi_{13.5}B_9Nb_3Cu_1$ (x = 1, 3, 5) alloys prepared by the melt-spinning technique has been performed. Nanocomposites composed of nanoscale $(Fe,Mn)_3Si$ magnetic phase embedded in an amorphous matrix were obtained by annealing their amorphous alloys at 535°C for 1 hour. The addition of Mn causes a slight increase in the mean grain size. The Curie temperatures of the initial amorphous phase and of the nanocrystals phase decreased, while the Curie temperature of the remaining amorphous phase remained nearly constant with increasing Mn content. Soft magnetic properties of the crystallized samples have been significantly improved by a proper thermal treatment. Accordingly, the giant magnetoimpedance effect is observed and ascribed to the increase of the magnetic permeability, and the decrease of the coercivity of the samples. The increased magnetic permeability is resulted from a decrease in the magnetocrystalline anisotropy and saturation magnetostriction.

Key words : microstructure, magnetic characteristics, magneto-impedance effect, thermomagnetic, nanocrystalline alloys

1. Introduction

The development of nanocrystalline $Fe_{73.5}Si_{13.5}B_9Nb_3Cu_1$ alloy, labeled as FINEMET, established a new approach to develop soft-magnetic materials with high magnetic flux density (B_s) in which the magnetocrystalline anisotropy can be reduced by refining the grain size in less than a few tens of nanometers [1]. This alloy exhibits attractive magnetic properties of 1.2-1.4 T for saturation magnetic flux density and high effective permeability (μ_e) [2], the mechanism of microstructural evolution in the FeSiBNbCu alloy and its applications have attracted much interests [3].

The origin of magnetic softening by reducing the grain size in the nano-scale range was explained by Herzer et al. [4] based on the so-called random anisotropy model. According to this model, when the grain size is smaller than magnetic exchange length (L_{ex}), the ultrasoft magnetic properties in the nanocrystalline materials are ascribed to average out the magnetocrystalline anisotropy due to the random distribution of the nano-scale grains. The roles of the elements for the nanocrystallization were indicated. It has been shown that the crystallization of Fe-Si-B-based amorphous alloys containing Nb and Cu causes the formation of nanoscale bcc structure and bcc alloys exhibit excellent ultrasoft magnetic properties. Ayers *et al.* [5] have proposed that Cu catalyzes the nucleation of the primary grains and Nb partitions to the grain boundary where it stabilizes the glassy phase that suppresses grain growth, leading to a ultrafine grain structure. Consequently, ultrasoft magnetic properties of $Fe_{73.5}Si_{13.5}B_9Nb_3Cu_1$ nanocrystalline alloy are obtained. Besides, the role played by Si and B mainly on the amorphicity of the alloy has been reported elsewhere [6], while the Fe content is responsible for the excellent high saturation magnetization.

Continuing efforts to improve the soft magnetic properties and the giant magneto-impedance (GMI) effect of FINEMET alloy have been made by modifying the alloy composition. Recently, some reports [7, 8] indicated an outstanding role of the Mn atoms in the evolution of exchange coupling between the crystalline and residual amorphous phases. Despite all these efforts, the detailed

*Corresponding author: Tel: +82-41-850-8276,
Fax: +82-41-850-8271, e-mail: heebok@kongju.ac.kr

correlation between the microstructure of these alloys, their magnetic properties and GMI behaviors is not well understood.

The objective of this work has been the systematic study of the influences of partial substitution of Fe by Mn in the $Fe_{73.5-x}Mn_xSi_{13.5}B_9Nb_3Cu_1$ (x = 1, 3, 5) alloys on the mirostructural and magnetic characteristics in conjunction with the GMI effect. The parallel evolution of the microstructure, magnetic properties and GMI behaviors is correlated.

2. Experiment

Amorphous ribbons with nominal composition $Fe_{73.5-x}Mn_xSi_{13.5}B_9Nb_3Cu_1$ (x = 1, 3, 5) of about 8 mm in width and 20 μm in thickness were produced from ingots using the standard single copper wheel melt spinning technique. In order to get the $Fe_{73.5-x}Mn_xSi_{13.5}B_9Nb_3Cu_1$ (x = 1, 3, 5) nanocomposites, the as-quenched amorphous alloys were annealed in vacuum for 1 hour at the temperature of 535°C.

The microstructure of the as-quenched amorphous ribbon and annealed ones was examined by X-ray diffraction (XRD Bruker D5005) with Cu-K_α radiation. A vibrating sample magnetometer (VSM DMS-880 Digital Measurement Systems) was used to measure magnetization as a function of the temperature for as-quenched alloys, with an applied field of 50 Oe and a heating/cooling rate of 4°C/min. An AC Permegraph (AMH-20) was employed to measure the room temperature permeability and coercivity of toroidal samples for both as-quenched alloys and annealed ones using the induction method.

Magneto-impedance (MI) effect was studied in the annealed samples. The samples with a length of about 15 mm were used for all measurements. The external dc magnetic field, applied by a solenoid, was swept through the entire cycle equally divided by 800 intervals from –300 Oe to 300 Oe. The frequency of the ac current was varied from 1 to 10 MHz, while its amplitude was varied from 10 to 30 mA. The schematic diagram of the experimental system can be found elsewhere [11].

The magnetoimpedance ratio (MIR) can be defined as $MIR(H)=\Delta Z/Z(H_{max})=1-|Z(H)/Z(H_{max})|$, where H_{max} is the maximum applied dc magnetic field. In present experiment H_{max}=300 Oe.

3. Results and Discussion

3.1. Microstrucral analyses

First, we examined the microstructure of the as-quenched samples by using X-ray diffraction (XRD) method.

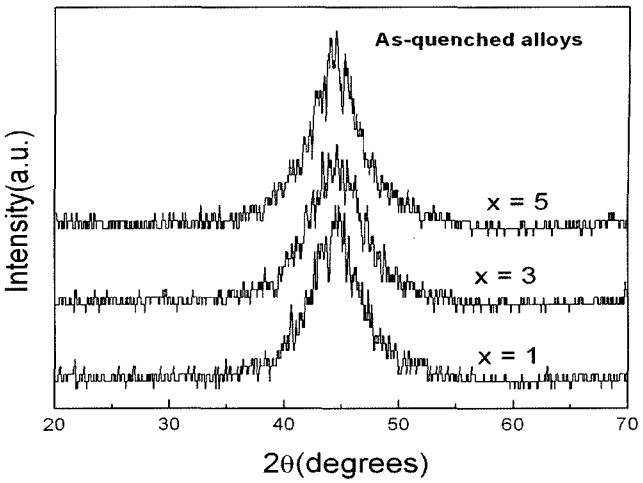

Fig. 1. XRD patterns of $Fe_{73.5-x}Mn_xSi_{13.5}B_9Nb_3Cu_1$ (x = 1, 3, 5) as-quenched amorphous alloys.

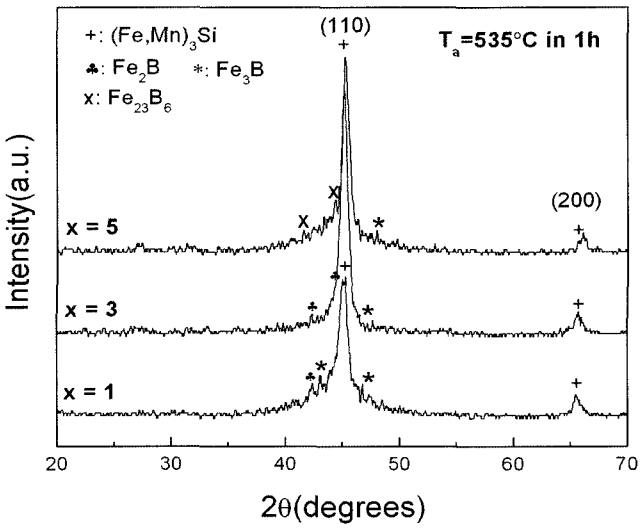

Fig. 2. XRD patterns of $Fe_{73.5-x}Mn_xSi_{13.5}B_9Nb_3Cu_1$ (x = 1, 3, 5) alloys annealed at 535°C for 1 hour.

As can be seen in Fig. 1, the XRD patterns of all as-quenched amorphous alloys exhibited only one broad peak around 2θ = 45°, which is often knows as a diffuse halo, indicating the amorphous nature of the prepared samples.

The nanocrystalline samples consisting of ultra-fine soft ferromagnetic phase dispersed in an amorphous matrix were obtained by annealing the precursor alloys at T_a= 535°C for 1 hour in vacuum. To confirm this, the microstructure of the nanocrystalline samples after annealing was examined by the XRD as shown in Fig. 2. It is clearly that, the $(Fe,Mn)_3Si$ soft ferromagnetic phase was detected in all investigated samples. This indicated that, upon a proper heat treatment, the as-quenched amorphous state was transformed into the ultra-fine $(Fe,Mn)_3Si$ grains

with excellent soft magnetic properties. Furthermore, the particle size, d, of $(Fe,Mn)_3Si$ grains can be determined from the breadth, B, of the X-ray diffraction peak, according to the Scherrer expression [12]:

$$d = \frac{0.9\lambda}{B\cos\theta_B} \quad (1)$$

Where λ is the X-ray wavelength (λ = 1.54056 Å), θ is the diffraction angle, and B is the full width at haft maximum (FWHM). Our calculations from the XRD patterns according to Eq. (1) revealed that, with increasing Mn content, the mean grain size of the samples were ~5.3 nm (x = 1), ~7.14 nm (x = 3), and ~7.51 nm (x = 5), respectively. These results suggest that the presence of Mn causes a slight increase in the mean grains size.

3.2. Magnetic characteristics

It has been well-established that there is direct correlation between structure and its changes upon thermal treatments and parallel evolution of magnetic properties.

3.2.1. Effect of Mn addition on the magnetic softness

First, the influences of partial substitution of Fe by Mn on the soft-magnetic properties of $Fe_{73.5-x}Mn_xSi_{13.5}B_9Nb_3Cu_1$ (x = 1, 3, 5) alloys, both as-quenched alloys and annealed ones, were investigated by the mean of magnetic hysteresis loops. It is found that the addition of Mn caused a decrease in the coercivity and the saturation magnetization for as-quenched amorphous samples (see Table 1). As examples displayed in Figs. 3a and 3b, the hysteresis loops of the amorphous samples (x = 1, 5) showed the squared hysteresis loops. This is likely related to the magnetoelastic anisotropy distribution due to the stress induced during the fabrication process. However, the hysteresis loops of the annealed samples have a typical form with improved soft magnetic properties. As shown in Table 2, the presence of Mn altered the magnetic softness and resulted in a decrease in the coercivity for the annealed samples, while initial permeability, maximum permeability increased. These are likely ascribed to a reduction in the magnetocrystalline anisotropy, and the saturation magnetostriction which is caused by a proper thermal treatment. In the nanocrystalline samples, the higher the Mn-doping content, lower the coercivity, and higher the permeability are obtained.

Table 1. Magnetic characteristics of as-quenched alloys $Fe_{73.5-x}Mn_xSi_{13.5}B_9Nb_3Cu_1$ (x = 1, 3, 5).

Sample	μ_i	μ_{max}	H_c (Oe)	M_s (emu/g)
x = 1	294	1940	0.2	133
x = 3	5,650	13,000	0.14	130
x = 5	1,200	9,800	0.14	128

3.2.2. Effect of Mn addition on the Curie temperatures

Next, we investigated the effects of Mn addition on Curie temperatures of samples by the thermomagnetic curves. Figures 4a and 4b show the thermomagnetic curves for the x=1 and 5 amorphous samples. As an example observed in Fig. 4a, as the temperature increased, the magnetization was abruptly reduced marking the

Table 2. Magnetic characteristics of annealed alloys (x = 1, 3, 5; T_a = 535°C for 1h) and the maximum MIR values, $(MIR)_{max}$ (%), measured at 2 MHz.

Sample	μ_i	μ_{max}	H_c (Oe)	M_s (emu/g)	MIR_{max} (%)
x = 1	17,000	32,000	0.037	142	65.4
x = 3	18,000	40,000	0.030	134	93.78
x = 5	41,000	58,000	0.023	129	128.72

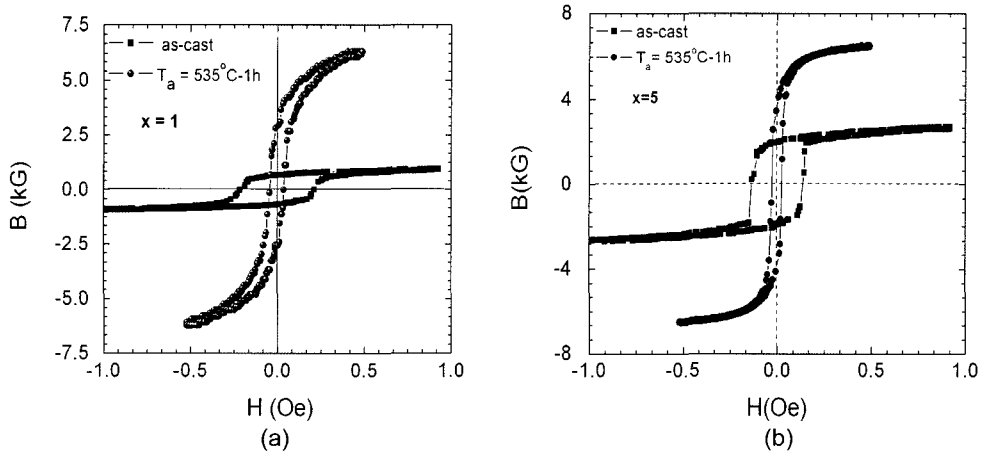

Fig. 3. Magnetic hysteresis loops of the (x = 1, 5) samples (both as-quenched and annealed at 535°C for 1 hour).

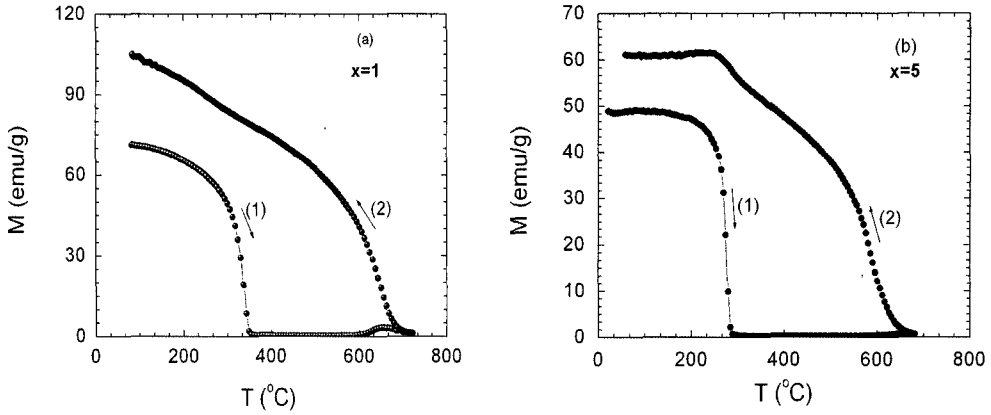

Fig. 4. Thermomagnetic curves of the $Fe_{73.5-x}Mn_xSi_{13.5}B_9Nb_3Cu_1$ (x = 1, 5) amorphous alloys: (1) heating curve and (2) cooling curve.

Curie temperature of the amorphous phase (T_{c1}) (see the heating curve (1)). With further increasing temperature, the magnetization is remained unchanged over a temperature interval up to a region where the crystallization of magnetic phases is occurred leads to an increase of the magnetization. The increase of the magnetization indicates the formation of some crystalline magnetic phase(s). In the cooling process with decreasing temperature (see the curve (2) in Fig. 4a), a large amount of $(Fe,Mn)_3Si$ grains are crystallized in the sample as indicated in XRD patterns (Section 3.1) leading to a strong increase of the magnetization. It is worth pointing out that the feature of the curve (2) in the cooling process is a typical two-phase material in which both phases are ferromagnetic but with different Curie temperatures. The first is a $(Fe,Mn)_3Si$ ferromagnetic phase with a high Curie temperature and the second is the residual amorphous matrix (Fe-Nb-B) with a lower Curie temperature. Simultaneously, a similar tendency was also observed in the x = 5 sample (see Fig. 4b). As can be seen in Fig. 5, the addition of Mn decreased the Curie temperatures of the initial amorphous phase (T_{c1}), of the nanocrystals (T_{c3}), whereas no noticeable variation in the Curie temperature of remaining amorphous phase (T_{c2}) was found. We indicate that the addition of Mn causes a slight increase the mean size of the grains. However, the grains are small enough, therefore, at elevated temperatures the magnetic properties of such material depend mainly on the crystalline content. It has been pointed out the use of DSC apparatus for estimating the crystallization fraction (χ_f):

$$\chi_f = \frac{\Delta H_a - \Delta H_t}{\Delta H_a} \qquad (2)$$

where ΔH_a and ΔH_t are crystallization enthalpies of as-quenched alloy and alloy annealed for time t, respectively.

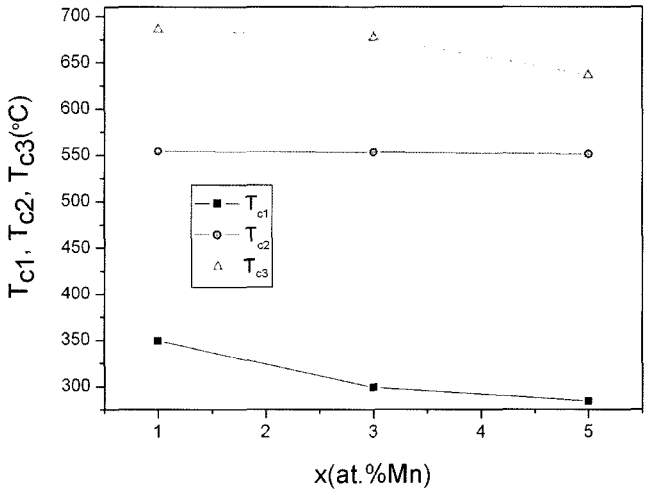

Fig. 5. Influence of Mn addition on the Curie temperatures of the initial amorphous phase (T_{c1}), the remaining amorphous matrix (T_{c2}), and the $(Fe,Mn)_3Si$ nanocrystals (T_{c3}).

Using expression (2) we derived the crystallization fraction of crystalline phase of $Fe_{73.5-x}Mn_xSi_{13.5}B_9Nb_3Cu_1$ (x = 1, 3, 5) alloys to be $\chi_f = 34\%$ (x = 1), $\chi_f = 56\%$ (x = 3), and $\chi_f = 72\%$ (x = 5). These results show that the volume fraction of crystallites is increased with Mn content substituted for Fe in Finemet, thus enhancing exchange coupling between grains leading to the improvement in soft magnetic properties of samples. It is interesting to note that the presence of Mn modified the microstructure and the Curie temperatures of precursor alloys in correlation with magnetic softness modifications.

3.3. Magneto-impedance analyses

Finally, to complete the analysis, the effect of Mn addition on the GMI effect was investigated. Recently, remarkable frequency- and field- dependence of the MI

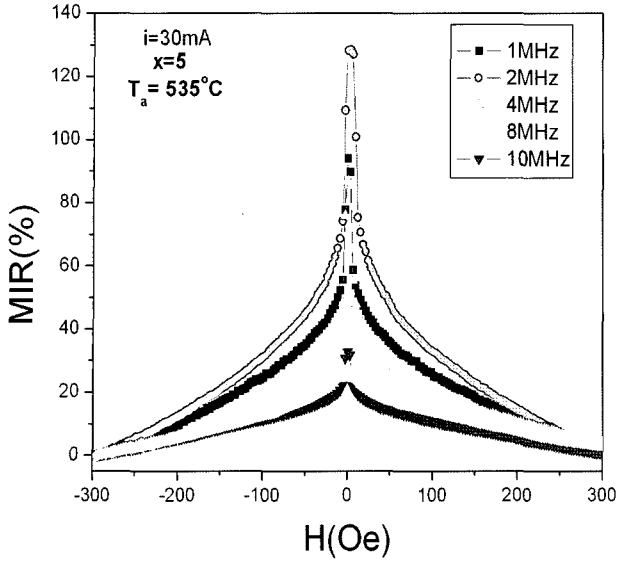

Fig. 6. MIR curves as a function of external dc magnetic field for the nanocrystalline sample (x = 5) measured at various frequencies up to f = 10 MHz.

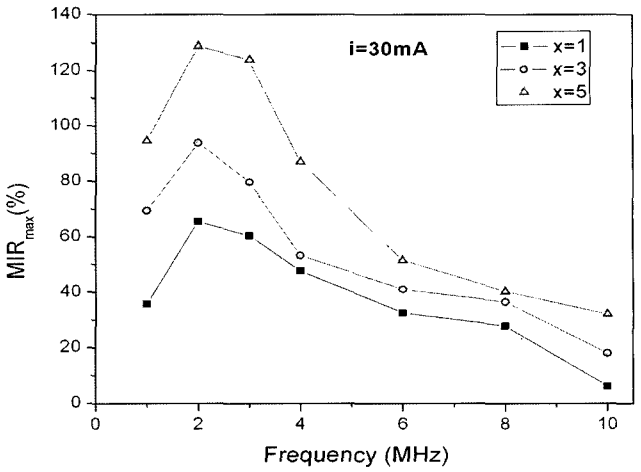

Fig. 7. The frequency dependence of the maximum MIR values of $Fe_{73.5-x}Mn_xSi_{13.5}B_9Nb_3Cu_1$ (x = 1, 3, 5) samples annealed at 535°C for 1 hour.

effect has attracted much interest because of its importance for applications in micromagnetic sensors and magnetic heads. In this study, the GMI profiles as a function of the longitudinal dc external magnetic field (H_{dc}) for all samples were measured at various frequencies up to f = 10 MHz. As an example, external dc magnetic field dependence of magnetoimpedance ratio (MIR) for the x = 5 sample annealed at 535°C in 1 hour is displayed in Fig. 6. It can be seen that the GMI profile exhibits a single-peak feature at near zero field ($H_{dc} \sim 0$) and the maximum value of MIR reached the highest value of 130% at a frequency of 2 MHz which is ideal for quick-response magnetic sensors. The higher MIR value observed at f = 2 MHz is likely due to the presence of its special domain structure as transverse domains formed by a magneto-mechanical coupling between internal stress and magneto-striction [9]. Accordingly, the frequency dependence of the maximum value of MIR for the all nanocrystalline samples (x = 1, 3, 5) is presented in Fig. 7. It is obvious that the GMI profile first increased with increasing frequency up to f = 2 MHz and then decreased at higher frequencies. These findings can be interpreted by adapting the model of the skin effect for thin ribbons [10]. According to this model, at low frequencies below 1 MHz ($a < \delta_m$, where a is the thickness of the ribbon and δ_m is the magnetic penetration depth), the MI effect is demonstrated to originate from the contribution of the induced magneto-inductive voltage to magnetoimpedance which is mainly ascribed from the circular magnetization process. As frequency increases, in the high-frequency regime when 1 MHz $\leq f \leq$ 4 MHz ($a \sim \delta_m$), the skin effect becomes dominant, the GMI effect can be interpreted in terms of the applied dc field magnetic field dependence of impedance as a result of the transverse magnetization with respect to the ac current direction flowing through the sample and the skin effect due to this ac current. In this frequency region, both the domain wall displacements and the magnetization rotation contribute to the change in the circular permeability and hence skin effect, consequently a higher MIR value was found. Beyond f = 4 MHz ($a > \delta_m$), the maximum MIR value decreases drastically with increasing frequency. It is believed that, in this frequency region ($f \geq 4$ MHz), the domain wall displacements were strongly damped owing to eddy currents thus contributing less to the transverse permeability, i.e., a small maximum MIR value.

Among the samples investigated, the largest GMI effect was observed in the nanocrystalline x = 5 sample. This is mainly due to the best magnetic softness in the sample, i.e., the decrease of coercivity and the increase of permeability (see Table 2).

4. Conclusions

The influences of Fe partially substituted by Mn on the microstructure and magnetic properties of $Fe_{73.5-x}Mn_xSi_{13.5}B_9Nb_3Cu_1$ (x = 1, 3, 5) alloys have been investigated, and the following conclusions were obtained:

a) The addition of Mn causes a slight increase of the mean grains size of soft ferromagnetic phase.

b) Soft magnetic properties of the nanocrystalline samples were significantly improved by a proper annealing treatment at 535°C for 1 hour.

c) The Curie temperature of the initial amorphous phase (T_{c1}) and of the nanocrystals (T_{c3}) decreased, whereas no noticeable variation in the Curie temperature of the remaining amorphous phase (T_{c2}) with increasing Mn content. This reflects the fact that Mn atom mainly exists in $(Fe,Mn)_3Si$ nanocrystals.

d) The largest GMI effect was observed in the nanocrystalline $x = 5$ sample among investigated samples because the softest magnetic properties was found in the sample. For this reason, the nanocrystalline 5 at% Mn-doping sample ($x = 5$) can be used for high-performance GMI sensor applications.

Acknowledgments

The authors wish to acknowledge the Center for Materials Science, National University of Hanoi (Vietnam) kindly supplied the samples. This work was supported by Korean Science and Engineering Foundation through Research Center for Advanced Magnetic Materials at Chungnam National University.

References

[1] M. Ohnuma, D. H. Ping, T. Abe, H. Onodera, K. Hono, and Y. Yoshizawa, J. Appl. Phys. **93**, 9186 (2003).
[2] Y. Yoshizawa, S. Oguma, and K. Yamauchi, J. Appl. Phys. **64**, 6044 (1988).
[3] M. E. McHenry, M. A. Willard, and D. E. Laughlin, Prog. Mater. Sci. **44**, 291 (1999).
[4] G. Herzer, IEEE. Trans. Magn. **25**, 3327 (1989).
[5] J. D. Ayers, V. G. Harris, J. A. Sprague, and W. T. Elam, J. Appl. Phys. **64**, 974 (1994).
[6] P. Martin, M. Vazquez, A. O. Olofijana, and H. A. Davies, Nanostruct. Mater. **10**, 299 (1998).
[7] C. G. Polo, J. I. Perez-Landazabal, V. Recarte, P. M. Zelis, Y. F. Li, and M. Vazquez,. J. Magn. Magn. Mater. **290**, 1517 (2005).
[8] A. C. Hsiao, M. E. McHenry, D. E. Laughlin, M. R. Tamoria, and V. G. Harris, IEEE. Trans. Magn. **37**, 2236 (2001).
[9] M. H. Phan, H. X. Peng, M. R. Wiscom, S. C. Yu, and N. Chau, Phys. Status Solidi A **201**, 1558 (2004).
[10] L. V. Pannia, K. Mohri, T. Uchiyama, and M. Noda, IEEE Trans. Magn. **31**, 1249 (1995).
[11] Heebok Lee, Y. K. Kim, K. J. Lee, and T. K. Kim, J. Magn. Magn. Mater. **215**, 310 (2000).
[12] B. D. Cullity, Elements of X-ray diffraction, 2nd Ed, Addison-Wesley Publishing Company, Inc., Reading, MA (1978), pp. 102.